



## Thermal and Flow Analysis of Different Shaped Pin Fins for Improved Heat Transfer Rate

Nhad K. Frhan Al-Abboodi<sup>1</sup>, Kamil Abdulhussien Khalaf<sup>1</sup>, Huda Ridha<sup>2\*</sup>, Mohammed G. Al-Azawy<sup>1</sup>

<sup>1</sup> Mechanical Engineering Department, College of Engineering, Wasit University, Wasit 52001, Iraq

<sup>2</sup> Veterinary Medicine College, Wasit University, Wasit 52001, Iraq

Corresponding Author Email: [hridha@uowasit.edu.iq](mailto:hridha@uowasit.edu.iq)

<https://doi.org/10.18280/ijht.400124>

### ABSTRACT

**Received:** 28 January 2022

**Accepted:** 25 February 2022

**Keywords:**

*fins configurations, fins profile geometric, CFD, Nu, Re, drag force*

In this paper, a micro pin fin heat sink is numerically investigated with four fins geometries (circular, elliptical, square, and drop shape) at two types of arrangement styles, inline and staggered arrangement. The hydrodynamic and thermal characteristics of different fin geometries and two arrangement styles have been compared under the exact value of Reynolds number and constant wall temperature thermal boundary conditions. The Reynolds number was sweeping in the range of (400-2800) to ensure the fluid flow velocity impact in the pin fin performance. The results obtained indicate that a longitude pin fin dropped with increasing Reynolds number at a distributed temperature. Also, the circular Pin fin reaches the lowest temperature comparison to the rest of the three-pin fin types. Generally, according to the extracted, Nusselt number for different geometries increased versus increasing the Reynolds number. Observe that the elliptical fin shape yields the highest Nusselt number at all Reynolds numbers. Moreover, the elliptical pin fin ejects the highest heat transfer rate, which indicates the pin fin performance. Furthermore, skin friction has a significant function with variation in Reynolds number.

## 1. INTRODUCTION

Microelectronic systems must be able to dissipate significant heat flux to maintain stable and optimal performance due to the rapid growth of today's electronic device production. Numerous ways have been developed to meet this need, including a micro channel heat sink with various fin shapes and arrangement styles. New and improved access will need to be considered to maintain the increasing trend the heat extraction. Because of their tiny mass and volume and more excellent surface-to-volume ratio, these heat sinks of the micro channel are ideal for cooling chips with high heat flux. Pin fins with various shapes and configurations have been presented to increase the cooling capacity and the temperature symmetry of this technology. Increasing the external heat dissipating area, which is extended surfaces, is one of the primary functions of the fins. The different pin fins and additional arrangements are used to enhance the micro heat sink's efficiency. Several investigation studies were found in the literature to truly comprehend a micro-pin fin heat sink's flow and heat transfer features. It was found that the most common pin fin shapes (round, elliptical, and square), as well as the staggered and inline configuration of the plate fins, amplifier the heat sink's ability to dissipate energy effectively. Staggered geometries outperformed inline in all circumstances, while elliptical fins performed best at a low-pressure loss and pumping power levels. Rounded pin fins work well at high power values, Feng et al. [1]. Pin fin heat sinks with fins in various forms (circular, square, and triangular) were empirically studied by Ricci and Montelpare [2]. According to their findings, triangle geometry was the best of the rest. Shaeri and Yaghibi [3] explored a flat plate with a flat array of solid and perforated fins and an incompressible air working

fluid based on the numerical simulation method. Compared to solid fins, longitudinal straight protruding fins have a remarkable heat transmission increase and a significant weight decrease. Micro square pin fin heat sinks with staggered configuration were explored by Ambreen et al. [4]. The authors use water for cooling with a Reynolds number varying from 60 to 800. Nusselt number and pressure loss rose with Re, but heat resistance dropped with pressure loss. It was found that the use of nanofluid in a micro pin fin heat sink had a positive influence on its performance. Investigated the effect of two nanofluids (diamond-water and Al<sub>2</sub>O<sub>3</sub>-water) for the heat sink with three types of pin fin geometry (square, triangular, and round) Mushtaq [5]. The results reveal that nanofluid improves thermal performance as well as lowers pressure. Moreover, the authors reported that circular fins have a greater heat transmission rate than the other fins. Yacine et al. [6] conducted a numerically study to evaluate the different pin fine geometry and fluid flow velocity effect on the pin fine's pressure losses, heat transfer coefficient, and temperature distribution. The computation fluid dynamic (CFD) solver using the k-ε turbulence model. The authors reported that the smaller spaces between the pin fins increase the pressure dropping, improve heat transfer, and maximize heat transfer rate, Baruah et al. [7] Performed a numerical study to analyze and investigate the heat transport rate for the solid and perforated elliptical pin fins in various applications. The elliptical pin fins are designed with three elliptical cross-section holes. The computational domains accounted for various intake velocities, different pressure, temperature, and velocity profiles. There is a significant improvement in heat transmission, while pressure decrease with the perforated fins over the solid elliptical pin fins. Ahmadian-Elmi et al. [8] conducted experimental studies to evaluate design parameters'

influence on airside thermal efficiency under combined natural and forced convection of the completely shrouded elliptical pin fin heat sinks. While, the thermal resistance of the heat sink is predicted using a theoretical model that incorporates geometrical, thermal, and flow characteristics. In mixed convection with helping flow, the overall heat transfer coefficient of the heat sink is indirectly measured using an experimental measuring approach. According to the author's result, the change of the geometry of the pin fin has a significant influence in the coefficient and the performance of the entire heat sink system.

Pressure and heat transport in a square pin-fin array experimentally studied by Jeng and Tzeng [9]. Numerical and experimental investigated the rectangular channel's flow and heat transfer properties implanted with pin fins. Compared to circular pin fins, drop-shaped pin fins had a lower aerodynamic loss because they effectively delayed or suppressed flow separation. The drop-shaped pin fins had a lower heat transfer enhancement than the circular pin fins. Drop-shaped pin fins offer a possible alternative to circular pin fins in particular performance metrics. The micro square pin-fin heat sink design was improved by Zhao et al. [10] based on computational studies of flow and heat transfer characteristics. Pin-fin porosity may be altered using a geometry-optimization technique to enhance cooling efficiency on a micro square heat sink. Nilpueng et al [11] conducted an experimental investigation to study pin fins geometry influence and the ratio between the center of the heat sink plate to the pin fin diameter. The authors involved three different pin fin profiles: square, circular, and 45° square pin fin, along with various pin fin diameters. The extracted result reveals that decreasing the space between pin fin results in the rise of the airflow interaction, leading to increased heat transfer dispersion and pressure losses.

The heat sinks with pin-fin for pure fluids were conducted extensively in the literature. Still, no study has been done on the four different fin geometries along with two different alignments (stagnation and inline configuration). The pin fin heat sinks are laid out inline and staggered to achieve the optimal heat sink void percentage and fin aspect ratio. Thermal efficiency data are determined for various parameters. The authors' best knowledge was to bridge this gap, which is the main aim of the present study. Inline and staggered configuration of a micro pin fin heat sink with four fin shapes (circular, elliptical, square, and drop shape) was examined quantitatively investigated in the current paper.

## 2. GEOMETRY MODELING

The Ansys Design workbench has modelled the pin fin heat sink. This analysis considered the following assumption;

- (1) An adiabatic tip for the fins.
- (2) The airflow direction is normal to the pin longitudinal.
- (3) Pin fin material is homogeneous and isotropic.
- (4) The modelling is three dimensions.

Electronic devices used heat sink in the heat ejection tactic. The working fluid medium is airflow and usually approaches an array of pin fin arrangements. The pin fin will be attached to a common surface of base plate. This paper investigates different pin fin geometry shape fundament at two type arrangement styles, inline and staggered arrangement.

### 2.1 Inline arrangement

First of all, the pin fin diameter is essentially considered a design parameter for the whole heat sink dimension, transverse pitch  $S_T$ , longitudinal pitch  $S_L$ , and the diagonal pitch  $S_D$  between tube centers. The following form dimensions the diagonal pitch:

$$S_D = \sqrt{S_L^2 + \left(\frac{S_T}{2}\right)^2} \quad (1)$$

The stream wise will approach the heat sink tub bank with velocity is  $V_{app}$ . Airstream penetrates the heat sink and owing to the narrow pipeline, and the airflow velocity will increase. The fluid flow in the diagonal region will be super-fast if the tube rows are very close to each other. Consequently, Reynolds Number will be influenced strongly. Reynolds number (Re) is dependent on the hydraulic wetted diameter and the heat sink maximum velocity  $V_{max}$ . For Inline arrangement, in minimum flow area between tubes, the maximum velocity will be accursed.

$$V_{max} = V \left[ \frac{S_T}{S_T - D} \right] \quad (2)$$

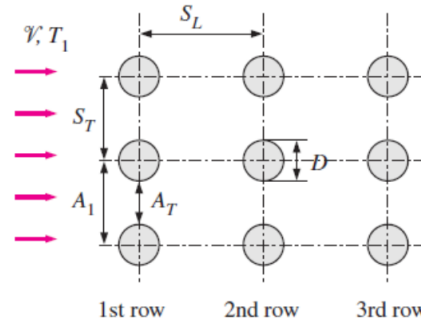


Figure 1. Circular pin fin inline arrangement

#### 2.1.1 Circular pin fin heat sink modelling

All four models have been designed through Ansys Workbench modular environment. Cylindrical pin fin heat sink computational domain is shown in Figure 2. The profile of the pin fin shape designed according to the Table 1.

Table 1. Circler: Geometry dimension parameter

Pin fin Number	$S_L$	$S_T$	Pin Fin Wet Diameter	Pin fin length
25	4 mm	4 mm	2 mm	50 mm

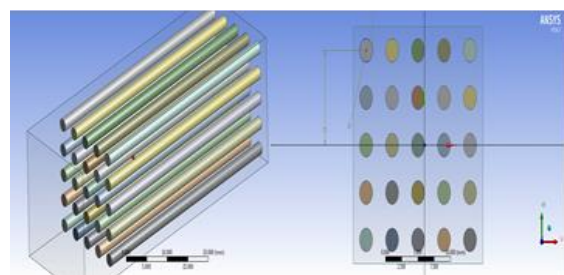


Figure 2. Circular pin fin geometry profile for the inline arrangement

The Circler pin fin was modelled by Ansys Workbench Design Modeler environmental and used the Ansys features advantage. Two of the zone will be constructing pin fin one of them, was stream represent the second zone each one with individual boundary condition. At the beginning inception with grate, a plane containing pin fin cross-section next step extrudes it through a z-direction to represent the pin fin sold body. The second plane will be generated to demonstrate the airflow zone and specify appropriate boundary conditions. Now two buddies are interfering with each other. This will confuse the meshing process, so function byline feature to separate them into two individual buddies. Finally, it will be coupled with Pin fin and wise stream in one particle buddy.

### 2.1.2 Elliptical pin fin heat sink

The elliptical pin fin configuration is shown in Figure 3 and Table 2.

**Table 2.** Elliptical: Geometry dimension parameter

Pin Fi Number	$S_L$	$S_T$	Major axis Diameter	Minor axis Diameter
25	5	4	4	2

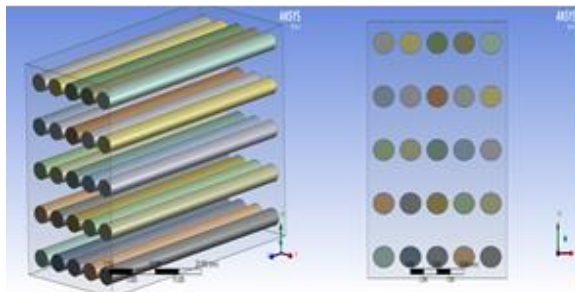


**Figure 3.** Elliptical pin fin geometry profile for the inline arrangement

### 2.1.3 Square pin fin heat sink

The square pin fin configuration is shown in Figure 4 and Table 3.

**Table 3.** Square: Geometry dimension parameter

Pin fin Number	$S_L$	$S_T$	Pin Fin Wet Diameter	Pin fin length
25	4 mm	4 mm	2 mm	50 mm

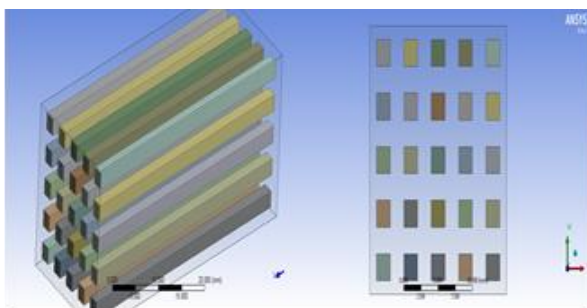


**Figure 4.** Square pin fin geometry profile inline arrangement

### 2.1.4 Drop shape pin fin heat sink

The drop pin fin configuration is shown in Figure 5 and Table 4.

**Table 4.** Drop: Geometry dimension parameter

Pin fin Number	$S_L$	$S_T$	Pin Fin Wet Diameter	Pin fin length
25	4 mm	4 mm	2 mm	50 mm

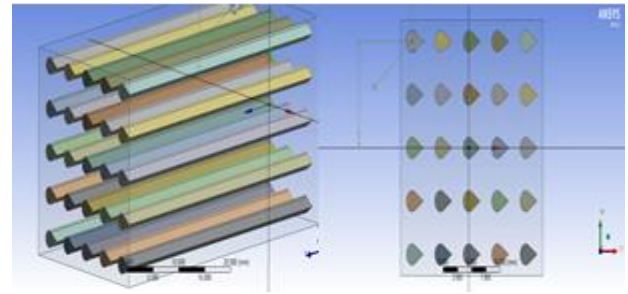


**Figure 5.** Drop pin fin geometry profile for the inline arrangement

## 2.2 Staggered arrangement

The fluid approaching through areas A1 and A2 will record maximum velocity through the region (Figure 6).

$$V_{max} = V \left[ \frac{S_T}{2(S_D - D)} \right] \quad (3)$$

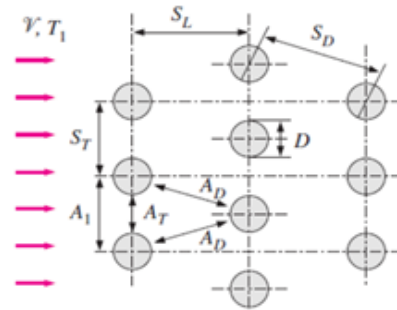


**Figure 6.** Circular pin fin staggered configuration

### 2.2.1 Circler pin fin heat sink modelling

The circular pin fin configuration is shown in Figure 7 and Table 5.

**Table 5.** Circular: Geometry dimension parameter

Pin Fin Number	$S_L$	$S_T$	$S_D$	Pin Fin Wet Diameter	Pin Fin Length
17	6 mm	6 mm	7 mm	2 mm	50 mm

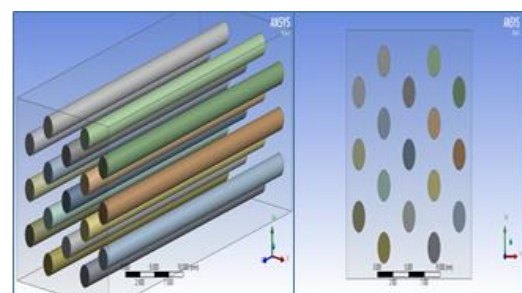


**Figure 7.** Circular pin fin geometry profile: Staggered arrangement

### 2.2.2 Elliptical pin fin heat sink domain

The elliptical pin fin configuration is shown in Figure 8 and Table 6.

**Table 6.** Elliptical: Geometry dimension parameter

Pin Fin Number	$S_L$	$S_T$	$S_D$	Major Wet Diameter	Minor Wet Diameter	Pin Fin Length
17	6 mm	6 mm	7 mm	4 mm	2 mm	50 mm

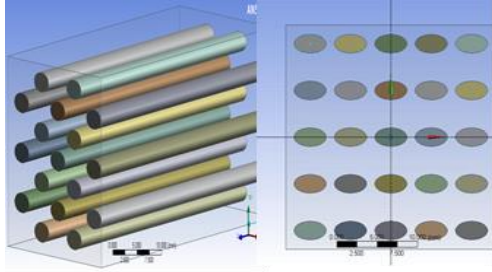


**Figure 8.** Elliptical pin fin geometry profile

### 2.2.3 Square pin fin heat sink domain

The square pin fin configuration is shown in Figure 9 and Table 7.

**Table 7.** Square geometry dimension parameter

Pin Fin Number	$S_L$	$S_T$	$S_D$	Pin Fin Wet Diameter	Pin Fin Length
17	6 mm	6 mm	7 mm	2 mm	50 mm

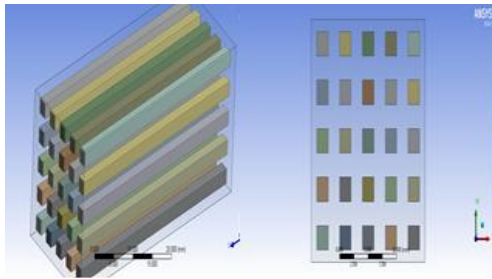


**Figure 9.** Square pin fin geometry profile

### 2.2.4 Drop shape pin fin heat sink

The drop pin fin geometry and configuration are shown in Figure 10 and Table 8.

**Table 8.** Drop geometry dimension parameter

Pin Fin Number	$S_L$	$S_T$	$S_D$	Pin Fin Wet Diameter	Pin Fin Length
17	6 mm	6 mm	7 mm	2 mm	50 mm

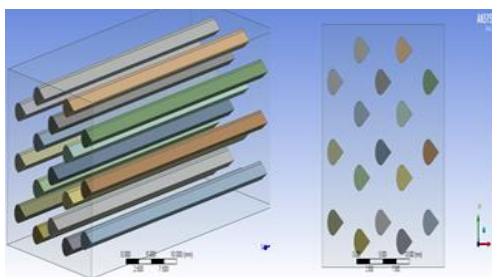


**Figure 10.** Drop pin fin geometry profile: Staggered arrangement

## 3. MATHEMATICAL FORMULATION

The velocity and temperature distributions are calculated by solving based on equations below [12] for the following three states: steady-state, 3-D, and incompressible laminar flow conditions.

The equation of Continuity is as follows:

$$\nabla V = 0 \quad (4)$$

The equation of Momentum is as follows:

$$\rho(V\nabla V) = -\nabla P + \nabla(\mu\nabla V) \quad (5)$$

The equation of energy is as follows:

$$\rho C_p (V\nabla T) = K\nabla^2 T \quad (6)$$

The model's boundary conditions are as follows: Temperatures and velocities were measured using finite values at the intake.  $T = 293 \text{ K}$ ;  $w = w_{in}$ ;  $u = v = 0$ ; Assumption that the flow has reached its maximum development at the discharge point:

$$\frac{\partial w}{\partial x} = v = u = 0, \quad \frac{\partial T}{\partial x} = 0 \quad (7)$$

As a result, the lower surface of the heat sink has a constant boundary state for the wall temperature ( $T = 373 \text{ K}$ ). For the model's other exterior surfaces (the right, left, and top walls), adiabatic walls are taken to be assumed:

$$\frac{\partial T}{\partial x} = \frac{\partial T}{\partial y} = 0 \quad (8)$$

Using the Reynolds number, it is possible to figure out the inlet velocity.

$$Re = \frac{\rho w_i D_h}{\mu} \quad (9)$$

$D_h$  is the diameter of the hydraulic. The pace at which a heat sink removes heat energy is known as the heat transfer rate:

$$q = m C_p \Delta T \quad (10)$$

It's also known as the variation between the inlet and exit pressures.

## 4. NUMERICAL SOLUTION

### 4.1 Fluent modelling

Computational Fluid Dynamics (CFD) is the numerical solution of the governing equation for fluid flow determined by inventiveness. Fluent goes through the solution across space or time to produce a numerical characterization of the whole flow field of interest. For example, the equation can be either steady or unstable. It can include in viscous and viscous flows, Compressive or Incompressible fluids, and fluid behavior that is non-ideal or reactive. The intended application determines the specific shape that is used. Using fluent

software to model heat transport and pressure drop in a heat sink and confirm the simulation with an analytical result, the study team hopes to advance the state-of-the-art in this area by removing geometrical complications. Fluent software has created several solutions and turbulence models for estimating Thermal Resistance, heat transfer, and other properties.

#### 4.2 Domain meshing

The heat sink system is embodied by two zones, fluid and solid. The airflow zone specifies the fluid domain and pin fin for the solid domain. The tetrahedral algorithms method is used to mesh the heat sink model. The physics preference was CFD, and the solver preference was fluent; the minimum size element was 0.0009. The total number of elements 890456 and nodes 48723 were manipulated to figure the grid in the heat sink case. There is a mesh metric parameter to check the meshing quality, orthogonal a listed under mesh measured control parameter. Orthogonal minimum quality value must be not more than 0.28 and maximum value not less than 0.98. Previously meshing quality limitation was applicable for all simulation cases Figure 11 shows CFD meshing model.

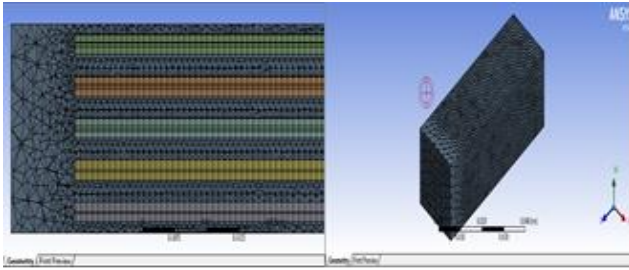


Figure 11. Heat sink pin fin meshing

#### 4.3 Fluent governing equation

Fluent, a commercial finite volume package is selected to analyze the model. Fluent has a governing equation for heat transfer and fluid flow depending on the conservation of mass, Energy, and Momentum. Fluent software will solve these equations. The geometry of circular, elliptical, square, and drop shape heat shape were illustrated in Figures 2-5, and Figures 7-10. In this analysis, the flow is simulating to 3D, laminar, incompressible and steady flow; crimped fin analysis is not considered radiation heat transfer and buoyancy. The following assumption is considered in the analysis.

1. Fluid is incompressible.
2. Properties are assumed to be constant.
3. The ambient temperature  $T_a$  is constant.
4. There are no heating sources throughout the pin fin heat sink. According to the previous assumption, the following basic equation is obtained under the steady state condition.

Continuity equation:

$$\frac{\partial u}{\partial x} + \frac{\partial v}{\partial y} + \frac{\partial w}{\partial z} = 0 \quad (11)$$

Momentum equation:

$$U \frac{\partial u}{\partial x} + V \frac{\partial v}{\partial y} + W \frac{\partial w}{\partial z} = \frac{1}{\rho} \frac{\partial p}{\partial x} + V \left[ \frac{\partial^2 u}{\partial x^2} + \frac{\partial^2 u}{\partial y^2} + \frac{\partial^2 u}{\partial z^2} \right] \quad (12)$$

$$U \frac{\partial u}{\partial x} + V \frac{\partial v}{\partial y} + W \frac{\partial w}{\partial z} = -\frac{1}{\rho} \frac{\partial p}{\partial x} + V \left[ \frac{\partial^2 v}{\partial x^2} + \frac{\partial^2 v}{\partial y^2} + \frac{\partial^2 v}{\partial z^2} \right] \quad (13)$$

$$U \frac{\partial u}{\partial x} + V \frac{\partial v}{\partial y} + W \frac{\partial w}{\partial z} = -\frac{1}{\rho} \frac{\partial p}{\partial x} + V \left[ \frac{\partial^2 w}{\partial x^2} + \frac{\partial^2 w}{\partial y^2} + \frac{\partial^2 w}{\partial z^2} \right] + g\beta(T - T_a) \quad (14)$$

Energy equation:

$$u \frac{\partial T}{\partial x} + v \frac{\partial T}{\partial y} + w \frac{\partial T}{\partial z} = \alpha \left[ \frac{\partial^2 T}{\partial x^2} + \frac{\partial^2 T}{\partial y^2} + \frac{\partial^2 T}{\partial z^2} \right] \quad (15)$$

#### 4.4 Boundary equation

Like the following, the boundary conditions are given. The range of the Reynolds number for the airstream inlet heat sink will vary from 400 to 2800; as a result, air speed will be changed. Inlet and outlet of the large space environment are 0Pa, the airstream inlet temperature is 25°C, and the heat transfer rate by conduction through the solid is equal to convection. The following equation represents the conduction through the solid pin fin.

$$\left[ \frac{\partial^2 T}{\partial x^2} + \frac{\partial^2 T}{\partial y^2} + \frac{\partial^2 T}{\partial z^2} \right] = 0 \quad (16)$$

In the numerical analysis, the temperature for the pin fin base plate  $T_{base} = 45^\circ C$  is assumed to be equal for the four different pin fin cross-section shapes. The side zone is modelled to be adiabatic with heat flux equal to zero.

#### 4.5 Converging calculation

The following Figure 12 shows how the calculation closes to the converging case that has been solved and involved in this paper. 200 iterations were taken three governing equations like energy equation, continuity equation, and momentum equation in the mode of velocity in x, y, z-direction. Post all the boundary conditions to the main parameters and take the laminar flow; the convergence will catch on 150 cyclic.

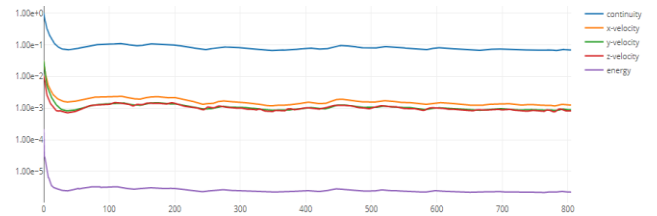
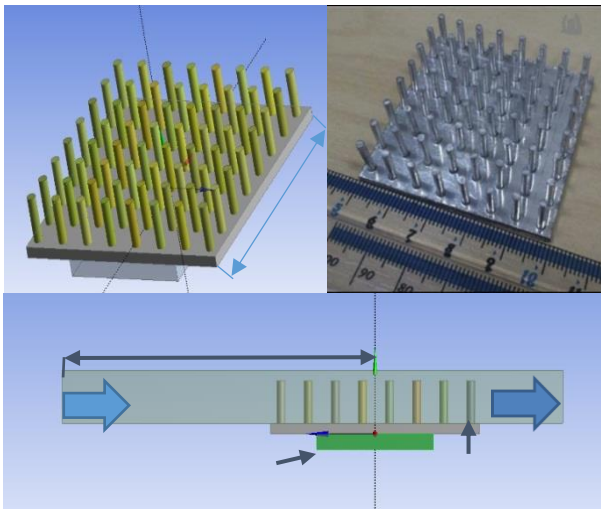


Figure 12. Solution convergent iteration diagram

### 5. CFD VERIFICATION AND VALIDATION MODEL

The pin fin sizes are dependent on the experimental heat sink design illustrated in Figure 13, which shows the heat sink

50 mm x 50 mm x 2 mm base plate, 6.5 mm pitch in both directions; the diameter of each pin was 2 mm  $\phi$  aluminum. Orientation of the heat sink in the straight channel segment, 110 mm from the upstream entrance to the channel. CFD mathematical model is used to analyze thermal airflow. Hydraulic diameter depends on the longitudinal scale when the intake air velocity varies between 6.5 and 12 m/s while the intake air temperature is maintained at 25°C. The airflow assumption was made for steady-state flow, incompressible and turbulent. As illustrated in Figure 1, the rate of heat conduction through the heat sink is balanced in the conjugate heat transfer model by the rate of heat convection into the airflow stream, which is achieved by using a coupled boundary condition at the solid-fluid surface interface. Along the bottom wall of the heat sink, a constant heat flux  $Q_i = 50W$ . A CFD mathematical model has been used to solve the full momentum and energy equation by approaching the Finite Volume Method-based code and using the second-order upwind. The CFD model is symmetrical along the channel sides, which helps reduce the mesh size density and time costs for solving the conjugate heat transfer model for pins aligned in the dominant flow direction.



**Figure 13.** (a) CFD model of pin fin heat sink; (b) empirical model of pin fine heat sink; (c) schematic diagram of the flow domain employed in CFD calculations

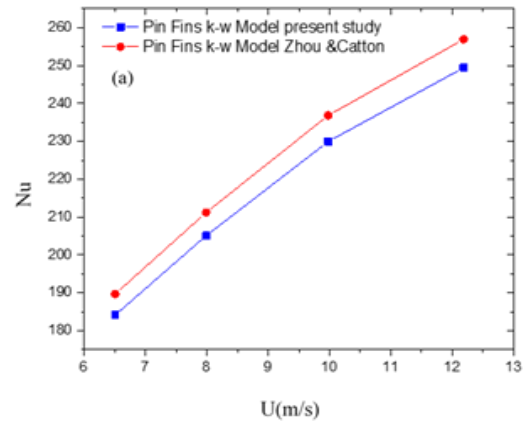
### 5.1 Study of grid dependency

On a series of grids for circular pin fins, numerical-based solutions to the conjugate heat transfer model are produced in the region depicted in Figure 13. The number of cells was varied between (745,000 to 785,000), while the grid resolution influenced the  $Nu_T$ ,  $T$ , and  $D_p$  demonstrated in Table 9. Increasing the cell number for the volume mesh more than leads to stable results in the range of less than 3%. All the results obtained from the present CFD model used these reliable grid refinement levels for the pin fin cases.

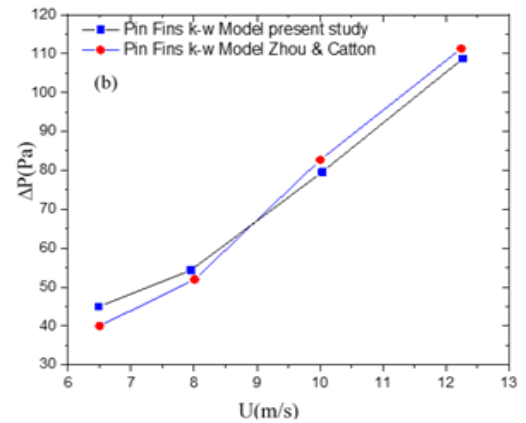
**Table 9.** Study of the grid independence for heat sinks pin fin

Number of cells	$Nu_T$	$T_{fin}$ (K)	$D_p$ (pa)
745,000	4.8	315	107.2
755,000	4.92	316	108
765,000	5.2	318	109
775,000	5.26	319	110
785,000	5.28	319.5	111

### 5.2 Verification and validation with previous reliable study



(a) Nusselt number,  $Nu$



(b) Pressure drops,  $D_p$

**Figure 14.** Comparison of predicted data with Zhou & Catton [13]

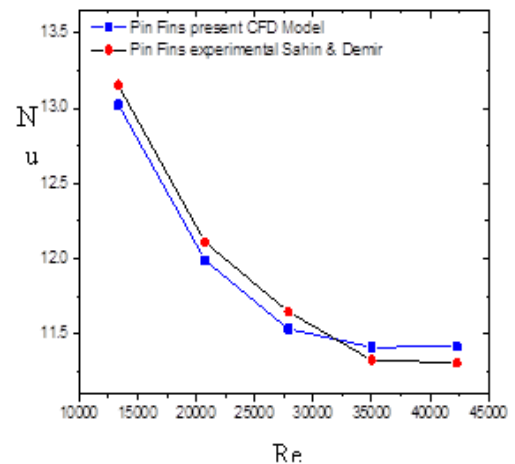


**Figure 15.** CFD Comparison of  $Nu/Nu_s$  predictions with experimental data of Sahin & Demir [14]

Figure 14 demonstrates the comparison of  $Nu$  and  $\Delta P$  predicted to result from CFD against the Zhou & Catton [13]. With average disparities of  $Nu$  and  $\Delta P$  of 2% and 4%, the findings are in good accord with those of benched Zhou and Catton [13]. Data from Sahin & Demir [14] (experimental study's) investigation on heat sink pin fins were comparable to the CFD model used in the current research. Figure 15 shows the comparison of CFD results of the  $(Nu/Nu_s)$  (where  $Nu_s =$

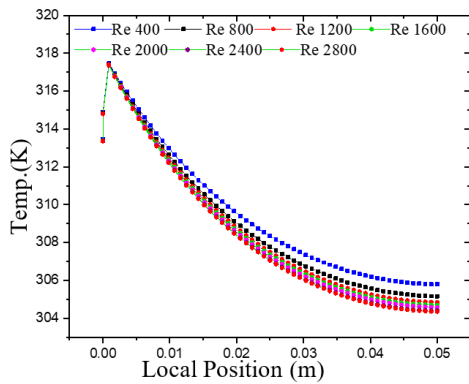
$0.77 RE^{0.716} Pr^{0.33}$  is the experimental correlation for Sahin & Demir [14] for heat transfer of the surface without pin fins. Again, the result was in good agreement against experimental data with less than 6% discrepancy.

## 6. RESULTS AND DISCUSSION

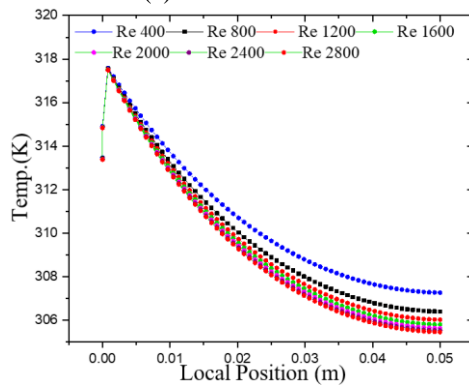
### 6.1 Temperature distribution over pin fin versa Reynolds number

#### 6.1.1 Pin fin heat sink inline arrangement

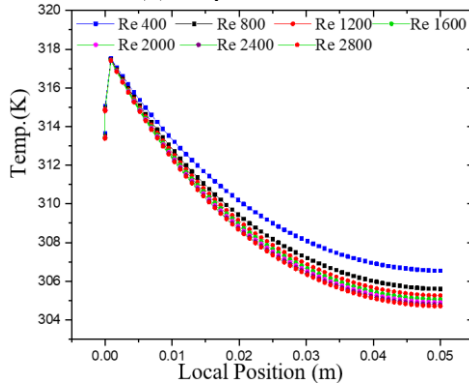
The Figures 16a, 16b, 16c, and 16d shows the precise relationship between the Reynolds number and the temperature distribution over Pin fin. It is clear from the results that increasing with Reynolds Number will be accompanied by a drop in the temperature. Also, the circular Pin fin reaches the lowest temperature compared to the other three pin fin shapes. Circular pin fin tip temperature equal to 317.9°C at 400 Re and drop to 304.1°C at 2800 Re is a good indicator for Pin fin performance relative to a longitude distribution temperature [15].



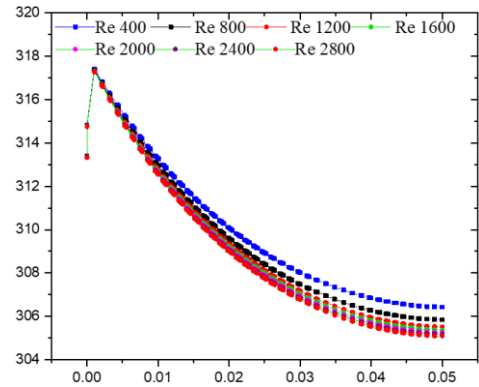
(a) Circular Pin fin



(b) Elliptical Pin fin



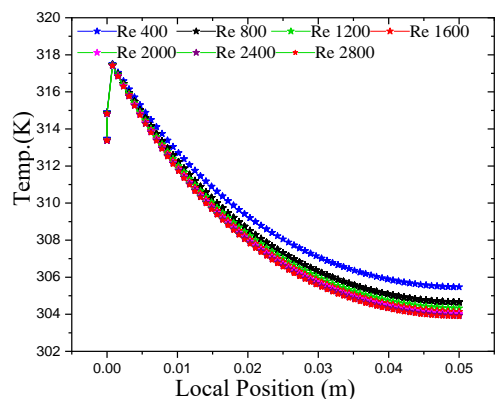
(c) Square Pin fin



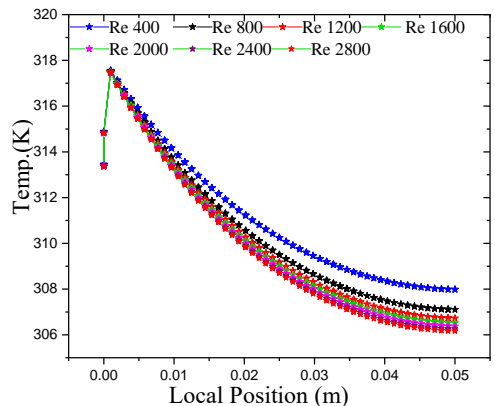
(d) Drop Shape Pin fin

Figure 16. Distribution temperature over pin fin staggered arrangement

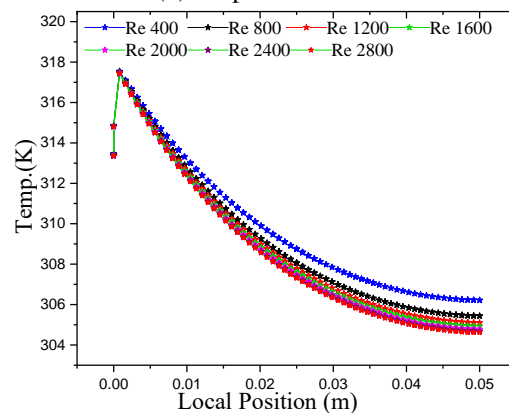
#### 6.1.2 Staggered arrangement of the pin fin heat sink



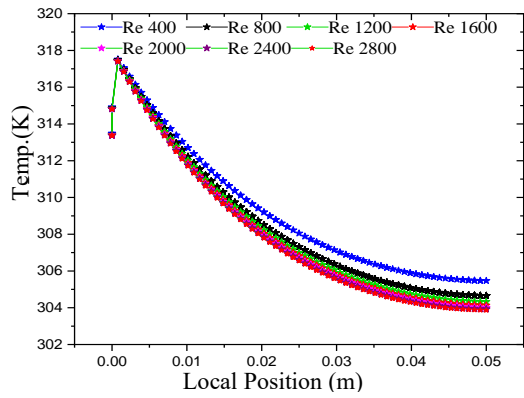
(a) Circular Pin fin



(b) Elliptical Pin fin



(c) Square Pin fin



(d) Drop Shape Pin fin

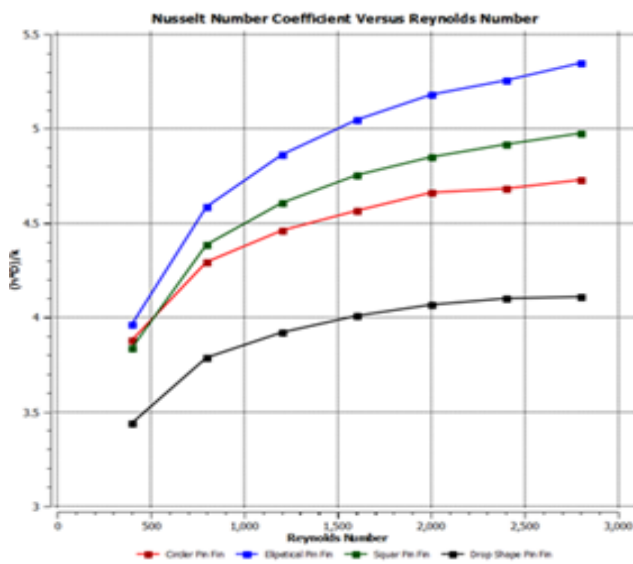
**Figure 17.** Distribution temperature over pin fin staggered arrangement

Figures 17a, 17b, 17c and 17d appears the precise relationship between the Reynolds number and temperature

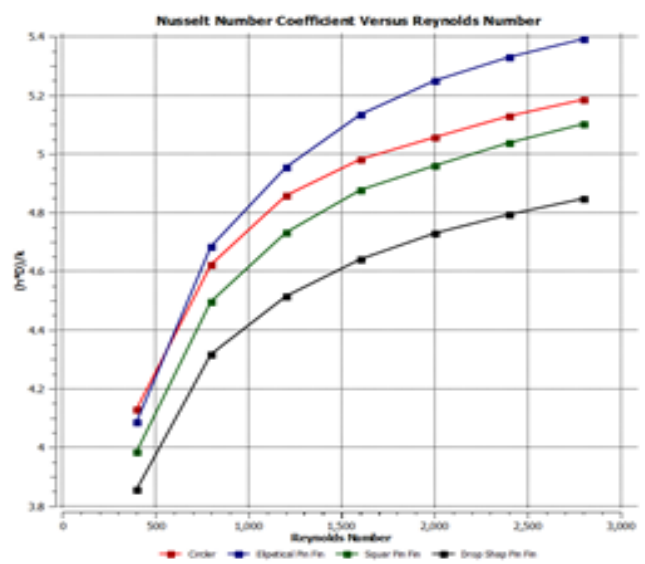
distribution over a longitude Pin fin. It increases with Reynolds Number leading to a drop in the distributed temperature. Also, the circular pin fin reaches the lowest temperature comparison to the other three pin fin shape. Circular pin fin tip temperature equal to 317.8°C at 400 Re and drop to 305.2°C at 2800 Re is a good indicator for Pin fin performance relative to distribution temperature.

## 6.2 Nusselt number versus Reynolds number

Heat transfer flux from heat sink depends primarily on pin fin arrangement configuration, Reynolds number, heat sink materials, finally, properties of incoming airflow. Nusselt number variation Versus Reynold number for various geometry represents in the following Figure 18. The results are grouped in two parts individually, inline and staggered arrangement. Generally, the comparison carried out the Nusselt number for different geometries versus variation on Reynolds number. It can observe that the elliptical fin shape yields the highest Nusselt number at all Reynolds numbers.

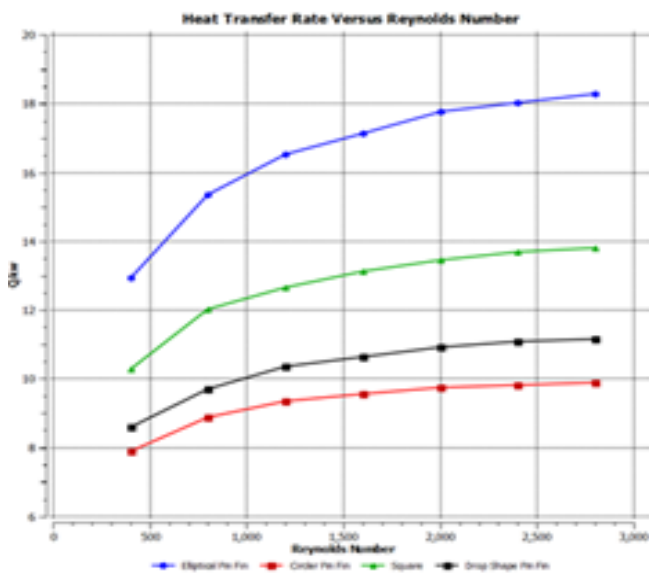


(a) pin fin inline arrangement

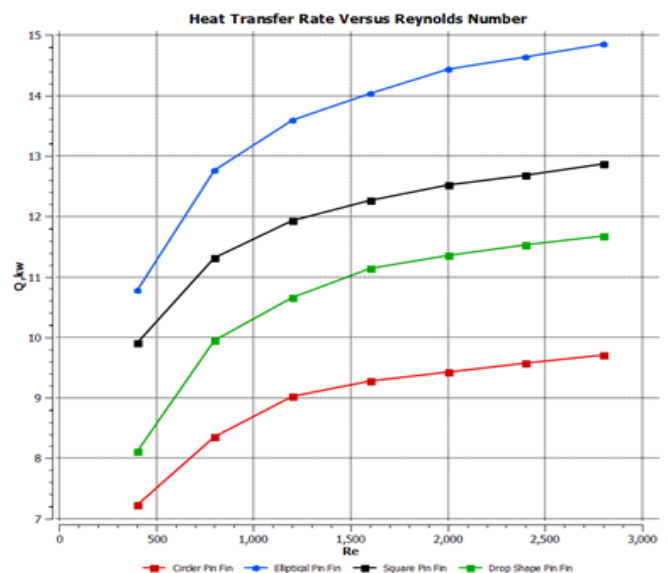


(b) Pin fin staggered arrangement

**Figure 18.** Nusselt number variation with Re for the inline and staggered arrangement



(a) Pin fin inline arrangement



(b) Pin fin staggered arrangement

**Figure 19.** Heat transfer rate variation with Re for the inline and staggered arrangement

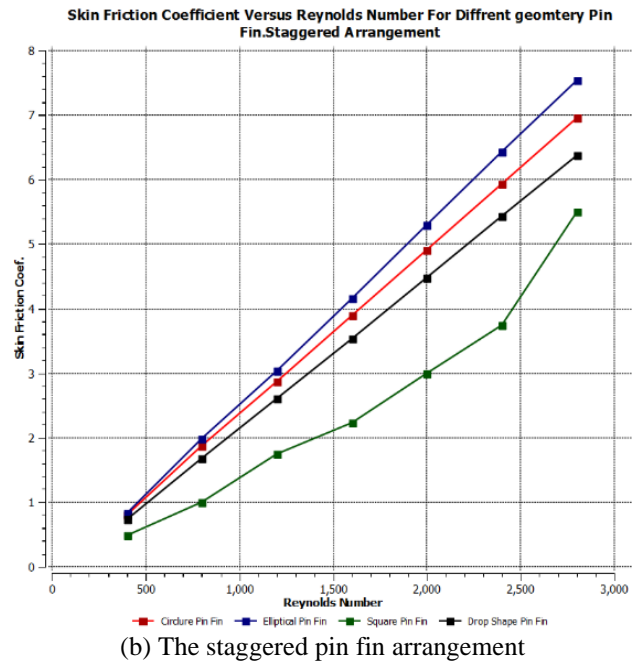
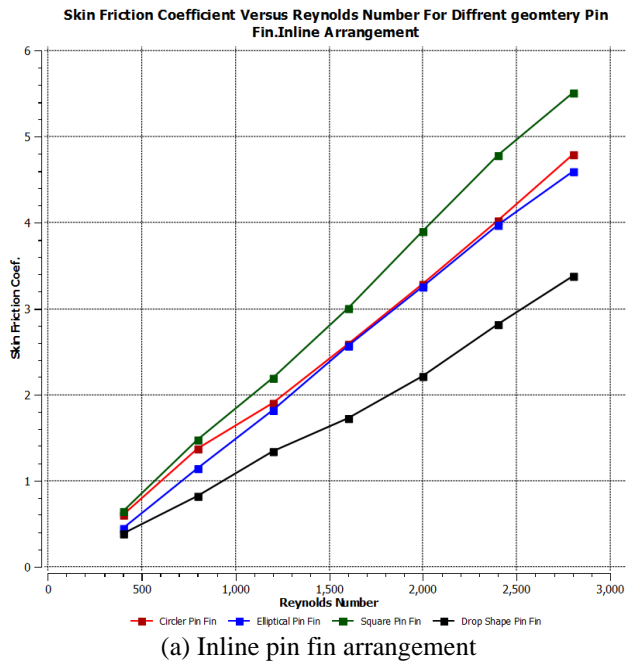


Figure 20. Drag pressure variation with Re for the inline and staggered arrangement

### 6.3 Heat transfer rate versus Reynolds number

A heat transfer manner identifies Nusselt number behavior for all four different geometries along with Reynolds number variation. Pin fin performance is depicted in Figures 19a and 19b by heat transfer rate. According to the results, the maximum heat transfer rate was (18.3 kW) at the (2800 Re). Another factor affects the rate of heat transmission in the outside surface area.[16]

### 6.4 Skin friction coefficient versus Reynolds number for different geometry pin fin

Skin friction depends on the body's geometrical orientation since it is a wall shearing stress parallel to the airflow. There is no friction at all on a surface that is perpendicular to the flow. To put it another way, because of the zero walls sharing stress, the idealized fluid flow has zero skin friction because of the strong relationship between friction and viscosity. Skin friction is the primary source of drag at low Reynolds numbers. Skin friction has a significant function with variation in Reynolds number. All the graphs tend sharply increase with Reynolds number. Figures 20a, and 20b shows the variation of the skin fraction for the different geometry profiles along with with the Reynolds Number (400-2800) for the inline and staggered arrangement. The result shows that the skin friction coefficient has an increasing trend with increasing Reynolds number. The maximum skin fraction was for the elliptical pin fin (7.5) at (2800 Re) for the staggered configuration.

### 6.5 Drag Pressure Coefficient versus Reynolds Number

In this case, the fluid is compelled to flow hit round surface at an appropriate high Reynolds number. The flow streamline will be detached from the surface body. Consequently, a low-pressure zone will be generated where recirculating and backflow occur, named the separation region.[16] Now the pressure drag depends on this separation area. A larger separation area means more significant drag pressure. Figures 21a and 21b shows the variations of the drag pressure with the

Reynold number and four different geometry profiles. Drag pressure has an increasing trend forward with increasing Reynolds number. The maximum drag pressure value was for the elliptical pin fin (0.2) at the (2800 Re) for the staggered arrangement.

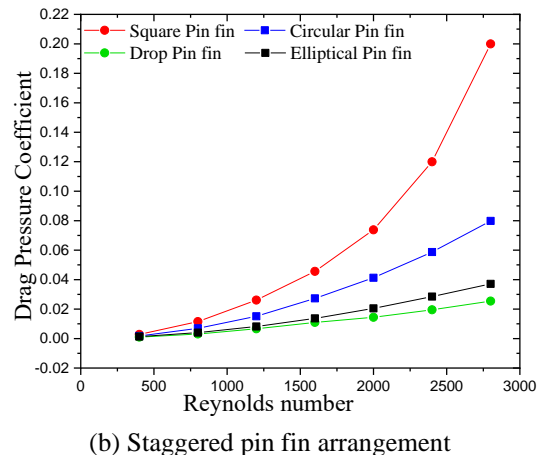
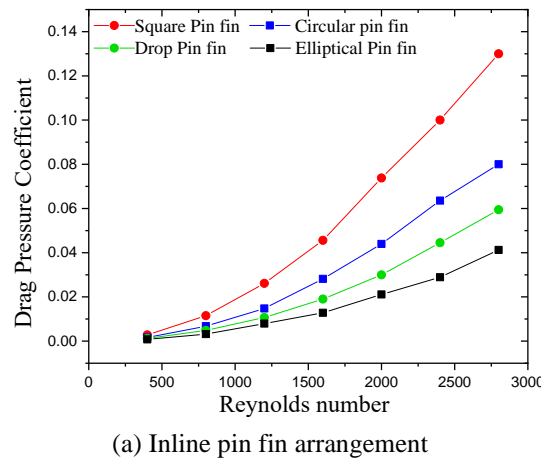


Figure 21. Skin fraction variation with Re for the inline and staggered arrangement

## 7. CONCLUSIONS

Four fins geometries (circular elliptical, square, and drop shape) were used in this research at two types of arrangement style, inline and staggered arrangement micro pin fin heat sinks exposed to constant wall temperature. The following observations may be drawn from the findings of this study:

1. The circular pin fin reaches the lowest temperature comparison to the other three pin fin shape.
2. The comparison carried out generally Nusselt number for different geometries versus variation on Reynolds number. The graph shows that the elliptical fin form yields the maximum Nusselt number at all Reynolds numbers.
3. The performance represented by heat transfer rate, elliptical fin shape eject highest rate of heat transfer flux. The other effect parameter influencing the heat transfer rate is exterior surface area.
4. Skin friction has a significant function with variation in Reynolds number. All the graphs tend sharply increase with Reynolds Number.
5. The pressure drag depends on this separation area, a more significant separation area means more considerable drag pressure.

## REFERENCES

- [1] Feng, Z.F., Hu, Z.J., Lan, Y.Q., Huang, Z.Q., Zhang, J.X. (2021). Effect of geometric of circular Pin – fins on fluid flow and heat transfer in an interrupted microchannel heat sink. *International Journal of Thermal Sciences*, 165: 106956. <https://doi.org/10.1016/j.ijthermalsci.2021.106956>
- [2] Ricci, R., Montelpare, S., (2006). An experimental IR thermo graphic method for evaluating the heat transfer coefficient of liquid-cooled short pin fins arranged in line. *Experimental Thermal and Fluid Science*, 30(2): 381-391. <https://doi.org/10.1016/J.EXPTHERMFLUSCI.2005.09.004>
- [3] Shaeri, M.R., Yaghoubi, M. (2009). Numerical analysis of turbulent convection heat transfer from an array of perforated fins. *International Journal of Heat and Fluid Flow*, 30(2): 218-228. <https://doi.org/10.1016/j.ijheatfluidflow.2008.12.011>
- [4] Ambreen, T., Saleem, A., Woo Park, C. (2019). Pin-fin shape-dependent heat transfer and fluid flow characteristics of water and nanofluids-cooled micropin-fin heat sinks: Square, circular and triangular fin cross-sections. *Applied Thermal Engineering*, 158: 113781. <https://doi.org/10.1016/j.applthermaleng.2019.113781>
- [5] Mushtaq, I.H. (2014). Investigation of flow and heat transfer characteristics in micro pin fin heat sink with nanofluid. *Applied Thermal Engineering*, 63(2): 598-607. <https://doi.org/10.1016/j.applthermaleng.2013.11.059>
- [6] Yacine Khetib, Y., Sedraoui, K., Gari, A. (2021). Numerical study of the effects of pin geometry and configuration in micro-pin-fin heat sinks for turbulent flows *Case Studies in Thermal Engineering*, 27: 101243. <https://doi.org/10.1016/j.csite.2021.101243>
- [7] Baruah, M., Dewan, A., Mahanta, P. (2021). Performance of elliptical pin fin heat exchanger with three elliptical perforations. *CFD Letters*, 3(2): 65-73. Retrieved from <https://www.akademiabaru.com/submit/index.php/cfdl/article/view/3337>.
- [8] Ahmadian-Elmi, M., Mashayekhi, A., Nourazar, S.S., Vafai, K. (2021). A comprehensive study on parametric optimization of the pin-fin heat sink to improve its thermal and hydraulic characteristics. *International Journal of Heat and Mass Transfer*, 180: 121797. <https://doi.org/10.1016/j.ijheatmasstransfer.2021.121797>
- [9] Jeng, T.M., Tzeng, S.C. (2007). Pressure drop and heat transfer of square pin-fin arrays in line and staggered arrangements. *International Journal of Heat and Mass Transfer*, 50(11): 2364-2375. <https://doi.org/10.1016/j.ijheatmasstransfer.2006.10.028>
- [10] Zhao, J., Huang, S.B., Gong, L., Huang, Z.Q. (2015). Numerical study and optimizing on micro square pin-fin heat sink for electronic cooling. *Applied Thermal Engineering*, 93: 1347-1359. <https://doi.org/10.1016/j.applthermaleng.2015.08.105>
- [11] Nilpueng, K., Mesgarpour, M., Asirvatham, L.G., et al. (2021). Effect of pin fin configuration on thermal performance of plate pin fin heat sinks. *Case Studies in Thermal Engineering*, 27: 101269. <https://doi.org/10.1016/j.csite.2021.101269>
- [12] Incropera, F.P., Dewitt, D.P. (1996). *Fundamentals of Heat and Mass Transfer*, fourth ed. Jhon Wiley and sons.
- [13] Zhou, F., Catton, I. (2011). Numerical evaluation of flow and heat transfer in plate-pin fin heat sinks with various pin cross-sections. *Numerical Heat Transfer Applications Part A: Applications*, 60(2): 107-128. <https://doi.org/10.1080/10407782.2011.588574>
- [14] Sahin, B., Demir, A. (2008). Thermal performance analysis and optimum design parameters of heat exchanger having perforated pin fins. *Energy Conversion and Management*, 49(6): 1684-1695. <https://doi.org/10.1016/j.enconman.2007.11.002>
- [15] Soodphakdee, D., Behnia, M., Copeland, D. (2001). A comparison of fin geometries for heat sinks in laminar forced convection: part 1 e round, elliptical and plate fins in staggered and inline configuration. *The International Journal of Microcircuits and Electronic Packaging*, 24(1): 68-78.
- [16] Deshmukh, P., Warkhedkar, R., (2013) Thermal performance of elliptical pin fin heat sink under combined natural and forced convection. *Experimental Thermal and Fluid Science*, 50: 61-68. <https://doi.org/10.1016/J.EXPTHERMFLUSCI.2013.05.005>